Melamine-based covalent organic framework-incorporated thin film nanocomposite membrane for enhanced osmotic power generation

Ralph Rolly Gonzales[1], Myoung Jun Park[1], Tae-Hyun Bae[2], Yanqin Yang[2], Ahmed Abdel-Wahab[3], Sherub Phuntsho[1,*], Ho Kyong Shon[1,*]

[1]Centre for Technology in Water and Wastewater, University of Technology Sydney, New South Wales, Australia

[2]School of Chemical and Biomedical Engineering, Nanyang Technological University, Singapore

[3]Chemical Engineering Program, Texas A & M University at Qatar, Education City, Doha, Qatar

*Corresponding authors: Email: Sherub.Phuntsho@uts.edu.au; Hokyong.Shon-1@uts.edu.au

Abstract

A melamine-based covalent organic framework (COF) nanomaterial, Schiff base network-1 (SNW-1), was incorporated into the polyamide layer of a novel thin film nanocomposite (TFN) pressure retarded osmosis (PRO) membrane. The deposition of SNW-1 was made on an open mesh fabric-reinforced polyamide-imide (PAI) support substrate through interfacial polymerization (IP). SNW-1 loading influence on the water permeability and osmotic power density during PRO operation was investigated. The porous and highly hydrophilic SNW-1 nanomaterial facilitated the flow of water molecules across the membranes, while maintaining satisfactory salt rejection ability of the polyamide selective layer. The membranes exhibited significantly enhanced surface hydrophilicity, water permeability, and power density. The mode of incorporation of SNW-1 during IP was also investigated and it was observed that the secondary amine groups of SNW-1 react with the carbonyl groups of 1,3,5-benzenetricarbonyl trichloride, the acyl halide precursor in polyamide formation; thus, SNW-1 was incorporated through the amine precursor, 1,3-phenylenediamine. Testing with 1.0 M NaCl as the draw solution, the TFN membrane with a loading of 0.02 wt% SNW-1 exhibited the highest water flux of 42.5 $Lm^{-2}h^{-1}$ and power density of 12.1 Wm^{-2}, while withstanding hydraulic pressure over 24 bar. This study suggests that COF-incorporation can be a promising method in PRO membrane fabrication to improve both osmotic performance and energy harvesting capability for the PRO process.

Keywords

Membrane; Pressure Retarded Osmosis; Thin Film Nanocomposite; Covalent Organic Framework; SNW-1

1. Introduction

Population, industrialization, and economy have all seen exponential growth, leading to a worldwide concern regarding environmental sustainability and climate change. The demand for clean water and renewable energy is therefore rising exponentially [1-5]. Desalination and wastewater reuse play significant roles in meeting the continuously increasing fresh water demand. However, current technologies such as thermal desalination and reverse osmosis (RO) are considered to be energy-intensive, thus not sustainable, despite recent efforts to significantly reduce energy consumption [6]. Thus, a desalination process which is less energy-intensive, less costly, and more environment-friendly needs to be developed. Aside from the high level of interest in fresh water production through seawater desalination and wastewater reuse, as a result of the alarming rate of fossil fuel depletion, there is also a significant surge in interest in non-conventional renewable energy, which include solar, geothermal, wind, and biomass [7-11].

Osmosis occurs through a semipermeable membrane, wherein water is transported from the less concentrated region (feed solution, FS) to the region with higher solute concentration (draw solution, DS) [12]. The membrane should be able to allow only water to pass through and retain most solute molecules or ions in each solution. Osmotic pressure (π) between the two solutions is the main driving force of osmosis. This natural phenomenon has been engineered to apply for a number of applications, including desalination, wastewater treatment, and osmotic power harnessing. The advantages of osmosis as a desalination technique are its low-energy requirement (as the process works using natural driving force), low cost, and low fouling propensity [13-15], unlike RO process which has to operate at high hydraulic energy.

Besides desalination, osmosis has also been engineered for generating osmotic power using the chemical potential difference by pressure retarded osmosis (PRO) [16-19]. The osmotic energy is generated due to the continuous pure water transport across the membrane thereby expanding the volume of the DS and when this happens in a closed restricted DS chamber, it can generate energy in the form of hydraulic pressure [16, 20-23]. The increased DS volumetric flow with high pressure can be used to run a hydro-turbine and this mechanical energy can be converted into electrical energy using a generator [7].

Power density is one of the most important parameter in determination of osmotic power generation viability by PRO process. When the available driving force (concentration differences) is fixed, membranes properties play a

significant role in the power density. Membranes with high power density are therefore more suitable for osmotic power generation; however, despite PRO process being a potential renewable energy process, the technology is yet to be fully commercialized.

Membrane properties such as permeability, selectivity, hydrophilicity and their robustness to fouling are some of the most important parameters for the power density of the membrane. Traditional polymeric membranes for osmotic processes are often limited since both water permeability and solute selectivity cannot be simultaneously improved, thus finding an optimal membrane fabrication method and membrane configuration still presents a challenge. Furthermore, membrane fabrication methods should also be environmentally-friendly and cost-effective. Recently, the synthesis of ideally thin, mechanically strong, highly water-permeable, and selective thin film composite (TFC) membranes for PRO process has been reported [24-27]. A number of studies have shown that improvement of the TFC membranes can significantly achieve higher water flux than the first generation of commercially-available membranes, the Hydration Technologies Inc.'s symmetric cellulose acetate membranes [28, 29].

TFC are composite membranes with a thick porous polymer substrate with a thin film of salt rejecting active layer made of polyamide. The membrane substrate for TFC PRO membranes are typically prepared first, followed by the *in situ* selective layer formation on the membrane substrate surface. Porous membrane substrate is normally casted on the nonwoven fabric by non-solvent-induced phase separation (NIPS) while the thin polyamide selective layer is formed by interfacial polymerization (IP) method [30]. A major factor that limits performance of PRO and any other engineered osmotic processes is the concentration polarization affects in the membrane. During PRO process, the support and selective layers of the membrane face the FS and DS, respectively. This is known as the PRO mode, or AL-DS membrane orientation, during which concentrative internal concentration polarization (ICP) may occur within the substrate. The osmotic driving force and resulting in significantly reduced water flux and power density [31]. Thicker membranes are associated with higher structural parameter and more severe ICP and therefore, the TFC PRO membranes must be designed to be of high porosity, strength, and minimum thickness.

One of the new approaches of fabricating osmotic membranes in order to enhance both permeability and selectivity is to incorporate nanomaterial as fillers into the membranes. Mixed matrix membranes (MMMs) consist typically of organic polymer bulk phase and the homogeneously dispersed inorganic particle phase [32-34]. These

MMMs have shown highly enhanced porosity, water permeability and selectivity compared to traditional polymer membranes. The filler nanoparticles affect the morphology, hydrophilicity and thus performance of the membrane. In conventional MMMs, porous inorganic materials are generally incorporated into the polymeric dope solution prior to membrane fabrication. Ideally, the addition of a small fraction of inorganic fillers may lead to a significant increase in overall water permeability and selectivity. TFN membranes, on the other hand, are prepared by incorporating the nanoparticles on the active polyamide layer instead of the substrate [35, 36]. Incorporation of nanomaterials into PRO membranes to form either MMMs or TFN membranes has shown enhancement in its porosity and hydrophilicity, leading to higher water flux and osmotic power during PRO process. Among the hydrophilic nanomaterials reported in literature are graphene oxide [37-40], zeolite [41], carbon nanotubes [42, 43], titanium dioxide [44, 45], and silica [46].

Recently, a new type of nanomaterial called porous coordination polymer (PCP) has been synthesized and used in the fabrication of membranes for various applications, such as gas separation, gas adsorption, ion exchange, drug delivery, catalysis, and liquid separation [33, 47-49]. Covalent organic frameworks (COF) and metal organic frameworks (MOF) are three-dimensional PCPs, which are currently receiving growing interest in the aforementioned research areas [50].

While MOF are comprised of metal ions and organic ligands forming a porous framework structure, COF are nano-sized diversified framework structured PCPs composed of light elements (C, H, N, O, and B) [51] in organic functional groups linked by covalent bonds, whose exceptional porosity, high surface area, and thermal stability make them highly advantageous compared to most inorganic nanomaterials for incorporation in membranes. Synthesis of COF, therefore, is a widely practical and promising field, especially now that there is an immense need for new materials that can be used for a wide variety of applications [47].

In this study, TFN PRO membranes were fabricated by incorporating lab-scale synthesized COF on the polyamide selective layer. The permeability, power density, porosity, and selectivity of the TFN membranes were evaluated in comparison to the conventional TFC membrane, as a function of COF loading rate. To the best of the authors' knowledge, no previous COF-incorporated TFN membranes have been prepared specifically for PRO application.

2. Materials and methods

2.1. Materials

Polyamide-imide (PAI, Torlon® 4000T-MV, Solvay, Republic of Korea) was used as the polymer material. Tetrahydrofuran (THF, 99.9%, anhydrous, Sigma-Aldrich, Australia) and N,N-dimethylformamide (DMF, 99.8%, anhydrous, Sigma-Aldrich, Australia) were used as the solvents for the polymer. Melamine (Sigma-Aldrich, USA), terephthalaldehyde (TA, Sigma-Aldrich, USA), dimethylsulfoxide (DMSO, Sigma-Aldrich, USA), THF, and methanol (MeOH, Sigma-Aldrich, USA) were utilized for nanomaterial synthesis. The following are the precursors for the selective polyamide layer: 1,3-phenylenediamine (*m*-phenylenediamine, MPD, 99%, Sigma-Aldrich, Australia) and 1,3,5-benzenetricarbonyl trichloride (trimesoyl chloride, TMC, 98%, Sigma-Aldrich, Australia). Heptane (99.9%, anhydrous, Merck, Australia) was used as the organic solvent for TMC and sodium chloride (NaCl, Chem-Supply, Australia) was used to evaluate PRO membrane performance. A 63 µm-thick polyester (PET, PETEX®, Sefar Pty Ltd, Australia) open mesh fabric was used as the support of the membrane substrate.

2.2. Schiff-based synthesis of SNW-1

The synthesis of the covalent organic framework SNW-1 was adapted and modified from previous studies [52, 53]. 6.26 g (49.7 mmol) melamine was solubilized in a mixture containing 10 g (74.6 mmol) g TA and 230 mL DMSO. The solution was degassed with argon and continuously heated at 180°C and stirred vigorously for 72 h under nitrogen atmosphere, at which formation of precipitates was observed. The solution was cooled down to room temperature and the precipitate was collected via vacuum filtration; after which it was washed with DMF and THF in succession, and finally purified using Soxhlet extraction with MeOH and THF. The yield SNW-1 precipitate was dried under vacuum conditions and temperature of 120°C for 24 h.

SNW-1 is an N-rich melamine-based COF nanoparticle which can be dispersed homogeneously in water and most organic solvents. It is a triazine-based framework, which is typically characterized by lower crystallinity and higher chemical and thermal stability [51]. Synthesized from melamine, composed of three exocylic primary amine functional groups, and TA, an industrial aldehyde, this particular nanomaterial has a number of amino groups which can provide reactivity, as well as hydrophilicity. The SNW-1 synthesized in this study exhibits a three-dimensional framework, with a particle size of 35-50 nm and major pore size of 5 Å, which is larger than the molecular size of

water (3 Å), but smaller than the typical seawater solute NaCl (5.64 Å). Covalent C-N bonds present in the monomeric products of TA and melamine link the monomers together to form the framework structure of SNW-1. This nanomaterial has BET and Langmuir specific surface area values of 725 and 965 m^2g^{-1}, respectively, and a total pore volume of 2.556 cm^3g^{-1}, due to a high degree of cross linking.

2.3. PRO membrane substrate casting

The PAI membrane substrates was first prepared by conventional NIPS. A 15 wt% PAI solution was prepared with DMF and THF (6:4 weight ratio) as solvents. The solution was stirred at 300-500 rpm at 60°C for 24 h. The solution was degassed and brought to room temperature prior to casting. The solution was poured onto the open mesh PET fabric attached on a glass plate and, using a casting machine (Elcometer 4340, Elcometer (Asia) Pte Ltd, Singapore), was spread into a film. The nascent membrane substrate was afterwards immersed in a water coagulation bath at 23-25°C to allow complete phase inversion, and afterwards stored in deionized (DI) water overnight to ensure complete removal of organic solvents.

2.4. Interfacial polymerization and SNW-1 incorporation

The selective polyamide layer was formed on one side of the PAI substrate through IP. Due to its stability both in aqueous and organic phases, various loading rates (from 0.01 to 0.1 wt%) of the SNW-1 were dispersed in both DI water and heptane, to prepare SNW-1-incorporated aqueous MPD and organic TMC solutions, respectively. Before soaking the membrane in both solution, solvents remaining on the surface were removed using air knife. The membrane substrates were first soaked in 2 wt% MPD aqueous solution for 2 min and then in 1.5 wt% TMC solution in heptane solution for 1 min. The excess TMC solution was drained and the membranes were dried in air for 3 min and oven-dried at 90°C for another 3 min. The prepared membranes were placed in DI water until tested.

The mode of incorporation of SNW-1 was first tested wherein a loading of 0.01 wt% of SNW-1 was used to prepare MPD and TMC solutions. The fabricated TFN membranes were denoted according to the COF-incorporation medium, i.e. TFN-M and TFN-T, for MPD and TMC, respectively. Upon comparing the morphology, characteristics, and performance of both membranes, the mode of incorporation at which a better performance was

observed was further used for the succeeding experiments, wherein the SNW-1 loading was increased from 0.01 wt% to 0.02, 0.05, and 0.10 wt%. A control TFC membrane was prepared without nanomaterial incorporation.

2.5. Membrane characterization

The membrane morphology and surface chemistry were characterized using a field emission scanning electron microscope (FE-SEM) [54] and Fourier transform infrared (FTIR) spectroscopy [55]. X-ray photoelectron spectroscopy (XPS, ESCALAB250Xi, Thermo Fisher Scientific, USA) was used to determine surface elemental composition. Surface roughness were analyzed by atomic force microscopy (AFM) using a scanning probe microscope (Dimension 3100, Bruker, Germany) operated on tapping mode (scanning area of 5 μm × 5 μm). Hydrophilicity was determined through contact angle measurements via an optical tensiometer (Attension Theta Lite 100, Biolin Scientific, Republic of Korea) with a built-in image processing software. Membrane thickness, water uptake ability, and porosity were measured similarly with a previous study [54].

2.6. Determination of membrane intrinsic transport properties and osmotic performance

The intrinsic membrane properties such as pure water permeability (PWP, A, L m^{-2} h^{-1} bar^{-1}), solute permeability coefficient (B), and structure parameter (S) of the tested PRO membranes were determined by conducting reverse osmosis (RO) test by applying hydraulic pressure of 10 bar over an effective membrane area of 19.5 cm^2, similar to a previous study by the authors [55]. Osmotic performance was tested using a bench-scale PRO system (Cheon Ha Heavy Industries Co. Ltd., Republic of Korea) similar to a previous study [23].

3. Results and Discussion

3.1. SNW-1 covalent organic framework material

FE-SEM was used to determine the size and characterize the synthesized SNW-1. Fig. 1 shows that the SNW-1 particles are spherical in shape, and each particle has a size of approximately 35-50 nm, making it possible to be incorporated in both the membrane substrate and polyamide selective layers, which are approximately 150 μm and

150 nm thick, respectively. The small size of the particles also allows it to be easily dispersed homogeneously in a solution.

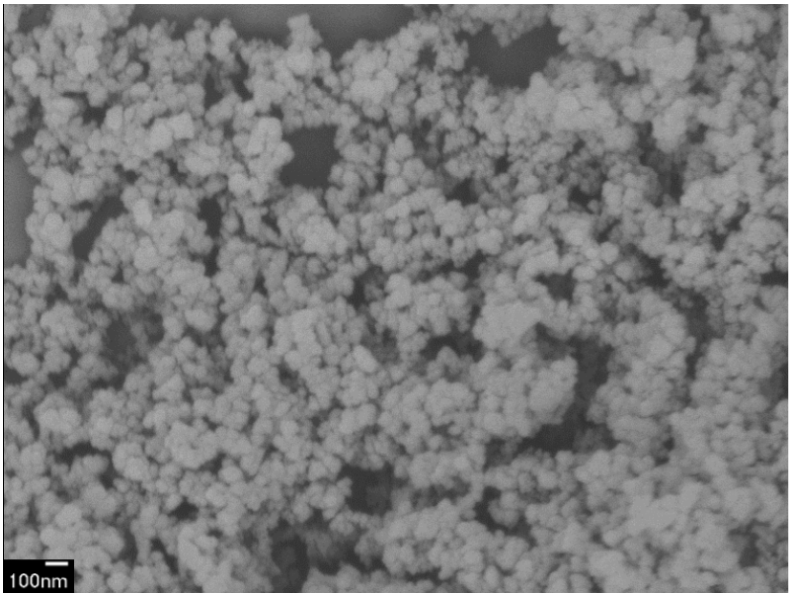

Fig. 1 FE-SEM image of the synthesized SNW-1 covalent organic framework nanoparticles

3.2. Mode of incorporation of SNW-1

One of the aims of this study is to determine the best way to incorporate the SNW-1 nanoparticles into the polyamide layer. The nanoparticles can be introduced onto the membrane selective layer through either one of the polyamide precursors. The MPD precursor is introduced onto the membrane surface through an aqueous solution, while TMC is dissolved in an organic solvent (i.e., heptane). SNW-1 both have hydrophilic (-NH) and hydrophobic groups (C=O and aromatic groups), that it is neither fully soluble in water nor in organic solvents, in fact it is stable in both and exhibited good dispersion.

The polyamide selective layer is formed from the reaction between the amine functional groups of MPD with the carbonyl carbon of acyl halide TMC [56]. Amines act as the nucleophile due to the presence of the lone electron pair on N, thus a nucleophilic attack on the carbonyl carbon occurs. The double bonds between C and O break, and the O atoms obtain a partially-negative charge, while N becomes partially positive due to the presence of four bonds on it. A proton is then transferred between N and O. The lone pair on the oxygen then forms the carbonyl C=O bond.

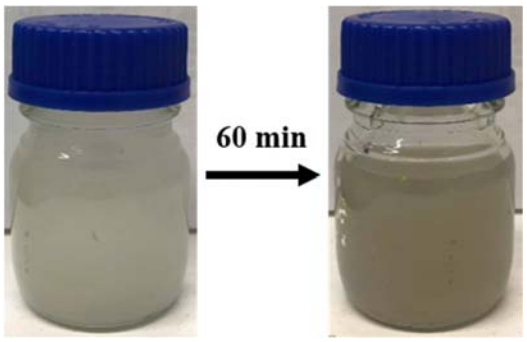

Fig. 2 The change in solution color of benzene-1,3,5-tricarbonyl chloride and SNW-1 after 60 min, indicating a reaction between the two substances.

SNW-1 is known to contain secondary amine (-NH) groups, which are also able to react with acyl halides to form amides. Upon dispersion of the COF nanoparticles, a similar nucleophilic substitution reaction between amine and carbonyl groups occurs and forms amide, albeit slowly. The dispersion solution of SNW-1 and TMC in heptane was initially clear; however, the solution turned milky gray as time passed (shown in Fig. 2). This is most likely due to the formation of amide from the reaction of SNW-1 and TMC.

To confirm the formation of amide, FTIR analysis was conducted on a membrane substrate wherein only the TMC solution with SNW-1 was contacted with the surface (sans MPD). The IR spectrum was then compared with that of a TFC membrane, whose polyamide is formed from the reaction of MPD and TMC, and as shown in Fig. 3, both exhibited similar peaks at 3185-3271 cm^{-1}, 1395-1440 cm^{-1}, and 1610 cm^{-1}, which all correspond to the presence of amide [57]. This confirms that the reaction of TMC and SNW-1 is highly similar to the polyamide polymerization reaction which occurs during IP.

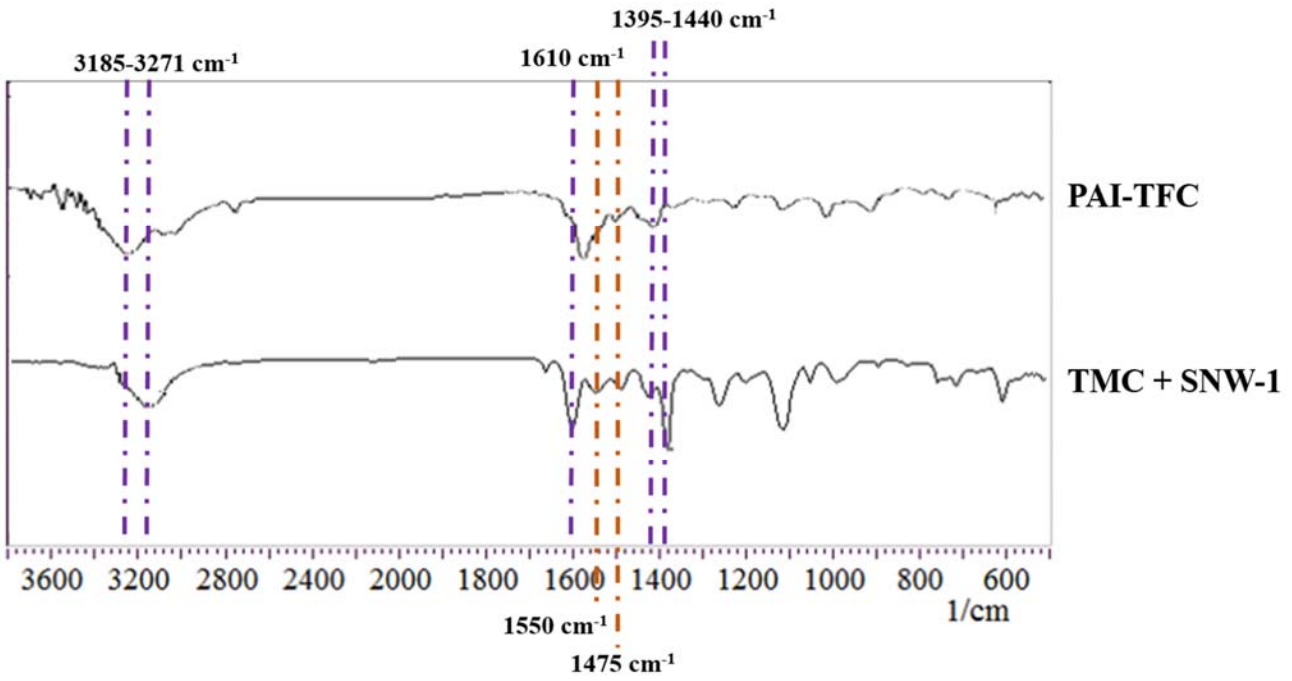

Fig. 3 FTIR spectra of (a) TFC polyamide and (b) product formed after the reaction of SNW-1 and benzene-1,3,5-tricarbonyl chloride.

While the SNW-1 COF nanomaterial is stable in both aqueous and organic phases, its reaction with TMC makes it not suitable to be incorporated through TMC during polyamide selective layer formation. The reaction between TMC and SNW-1 is similar to that of the polymerization reaction during IP, due to SNW-1's secondary amine groups. Nucleophilic substitution of amine occurs at the carbonyl carbon of TMC, leading to the formation of amide groups. Mixing TMC and SNW-1 together will then effectively react in solution, decreasing the integrity of the TMC solution prior to formation of polyamide during IP. Therefore, MPD was chosen as the mode of incorporation of SNW-1 in PRO TFN membrane preparation.

3.3. TFC and TFN membrane characterization

The surface chemical composition of the TFC and TFN membranes were characterized using FTIR spectroscopy; the spectra of the membrane surfaces are shown in Fig. 4. The TFC membrane showed absorption peaks at 3271 cm^{-1}, 1440 cm^{-1} and 1610 cm^{-1}, which are indicative of the carbonyl group of an amide functional group, showing

that polyamide formation via IP was successful. The peaks around 1440 cm^{-1} and 1610 cm^{-1} are likewise visible in the spectra of these membranes; however, the peak at 3271 cm^{-1} was not visible in the TFN membrane spectra, which show that the intensity of the hydroxyl group peak decreased upon incorporation of SNW-1. This can be attributed to the electrostatic interactions that occurred between the polyamide precursors and the COF nanoparticles [58]. Additional peaks at 1475 cm^{-1} and 1550 cm^{-1}, which are characteristic of the triazine group of SNW-1 [52], indicating that SNW-1 is incorporated into the polyamide layer.

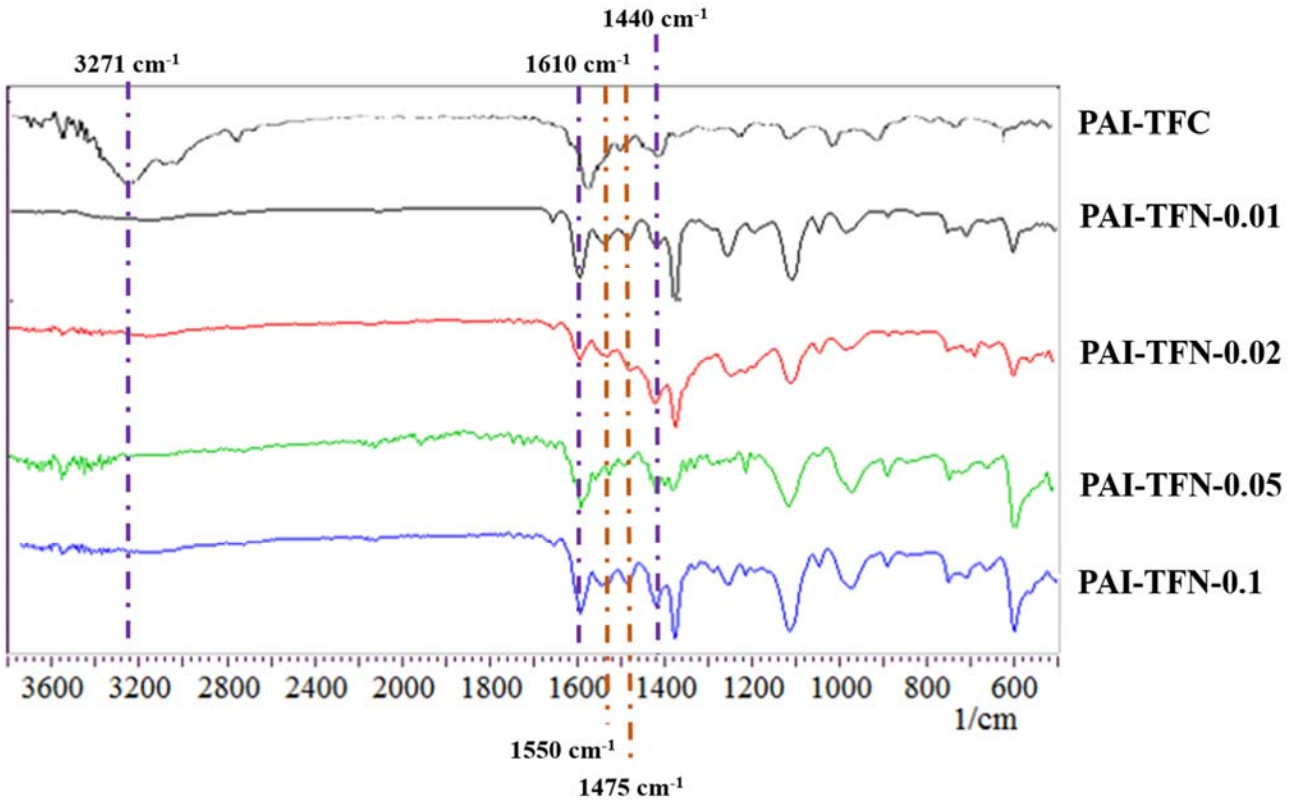

Fig. 4 FTIR spectra of the TFC and TFN membranes.

Aside from determination of the functional groups present in the membrane surfaces using FTIR spectroscopy, elemental analysis of membrane surface was also performed using XPS. XPS spectra of the TFC and TFN membranes are shown in Fig. 5a. To provide a simpler comparison, the TFN membranes with the lowest and highest SNW-1 loadings were chosen as the representative samples for XPS analysis. Chemical composition values of carbon, nitrogen, and oxygen, were shown in

Table 1. The XPS results indicate that nitrogen content further increased with the presence of the SNW-1 COF nanoparticles, with TFN-0.1 having the highest % N (14.04 %), confirming the successful incorporation of SNW-1 in the polyamide selective layer. Fig. 5 also shows the resolved N1s peak of the TFN membrane. The TFN membrane exhibits peaks at 396.18 and 402.48 eV binding energies, corresponding to C-N-C and H-N-C=O, which both correspond to the groups found in polyamide. A peak at 399.78 eV, that corresponds to C=N-C present in the triazine structure of SNW-1 [52], is also found, indicating the presence of SNW-1 in the TFN membrane.

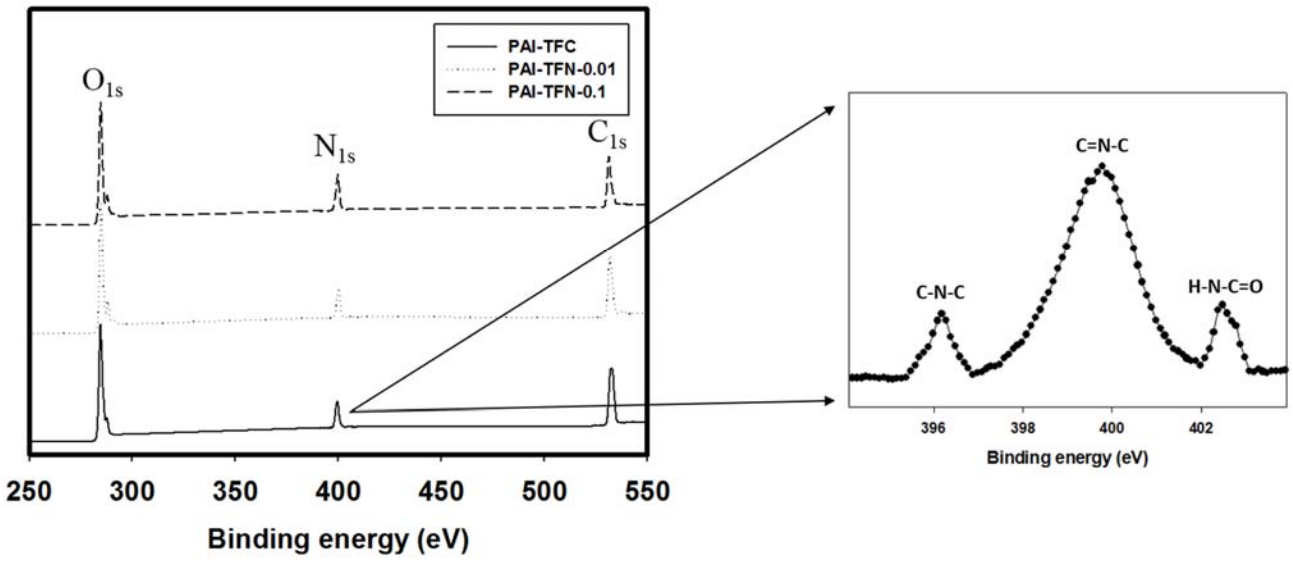

Fig. 5 XPS spectra of the TFC and TFN membranes.

Table 1 Chemical composition of the TFC and TFN membrane surfaces.

Membrane	C (%)	N (%)	O (%)	Others (%)
TFC	71.83	9.59	17.88	0.70
TFN-0.01	73.68	11.31	14.55	0.46
TFN-0.1	72.72	14.04	12.70	0.54

The membrane surface and cross-section morphology were analyzed using FE-SEM, as shown in Fig. 6 and **Error! Reference source not found.**. Polyamide, typically characterized by ridge and valley structures, was formed on top of the PAI substrate, as seen from Fig. 6 [59]. This signifies that since the SNW-1 nanoparticles

are incorporated with the TMC solution, the particles remained mostly on the surface, and not embedded in the polyamide layer. This change in morphology of the polyamide layers of the TFN membranes may play a major role in modifying other properties of the membranes, i.e. porosity, roughness, hydrophilicity, water permeability, and selectivity. The top and bottom surface, as well as cross-section, SEM images (**Error! Reference source not found.**) show that the TFC and TFN membranes exhibit a mixture of sponge-like and finger-like porous structures.

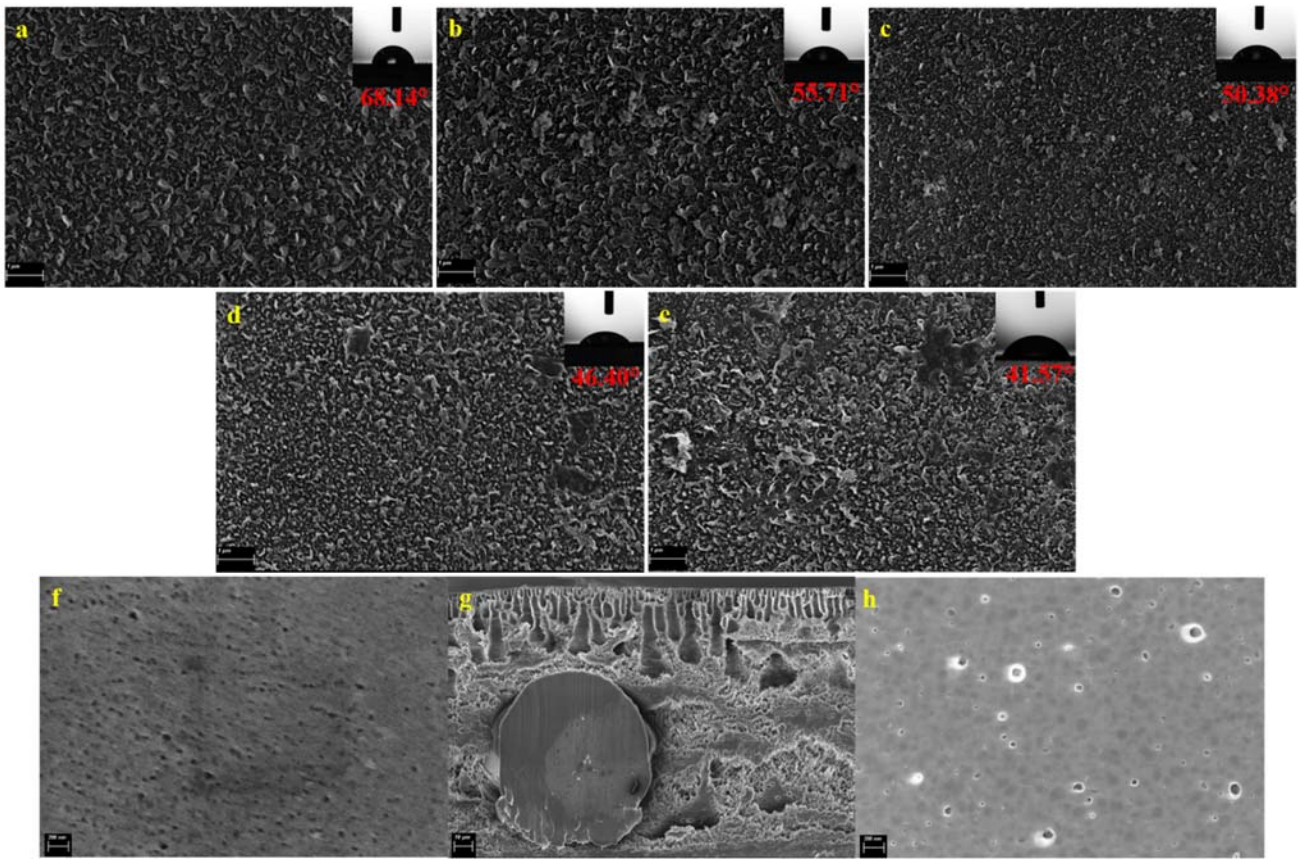

Fig. 6 Surface morphologies of the (a) TFC, (b) TFN-0.01, (c) TFN-0.02, (d) TFN-0.05, (e) TFN-0.01 PRO, (f) substrate top surface, (g) substrate cross section, and (h) substrate bottom surface membranes, respectively, taken through FE-SEM imaging. Contact angle measurements of each membrane were also included inset.

One of the direct effects of incorporation of SNW-1 on the polyamide layer is the enhanced surface hydrophilicity and affinity to water. Furthermore, enhanced surface hydrophilicity is integral in the improvement of water flux of PRO membranes [60]. To be able to evaluate surface hydrophilicity of the membranes, static water

contact angle was measured. However, contact angle is not only a function of hydrophilicity, but also surface smoothness [38], wherein smoother surfaces normally have lower contact angles. As seen from Fig. 6, the water contact angle measurements at the membrane surface were observed to decrease slightly as the nanomaterial loading increased. Polyamide has both hydrophobic carbonyl (C=O) and hydrophilic N-H groups, making the TFC membrane selective layer exhibit properties of both. Upon incorporation of SNW-1, the amine groups of SNW-1 further react with TMC and form amide groups, resulting the membranes to exhibit low hydration energy and have more affinity with water. Incorporation of the porous and hydrophilic SNW-1 would have definitely improved the overall hydrophilicity of the membranes; however, the contact angle differences were not significantly high. This is because incorporation of the nanomaterials also resulted in increased surface roughness as most nanoparticles are exposed to the surface of PA layer [61]. Overall, there were considerable improvements observed in hydrophilicity in the membranes after the selective polyamide selective layer formation on the PAI substrate and the subsequent incorporation of nanomaterials. The relative hydrophobicity and low surface energy of PAI caused the high contact angle measurement observed for the substrate [54]. The observed increase in the surface hydrophilicity after incorporation of SNW-1 is due to the presence of the secondary amine functional groups (-NH) left unreacted with TMC [52].

Membrane surface roughness was characterized by AFM analysis. Fig. shows the three-dimensional AFM images of the membrane surfaces for the TFC and TFN samples. The mean roughness (R_a, nm) and root mean square ridge elevation (R_{ms}, nm) are also presented. The R_a and the R_{ms} of 8.16 nm and 10.4 nm, respectively, were observed for the TFC membrane. The R_a values were seen to increase as the loading of the nanomaterial increased. However, the R_{ms} values did not follow the same trend and most likely these values were influenced by the size of the nanoparticles embedded on the surface. It is also noteworthy that the TFN-T membranes exhibited higher surface roughness than their TFN-M counterparts, as seen by the AFM images which show agglomeration of the COF nanoparticles, hereby increasing the overall roughness.

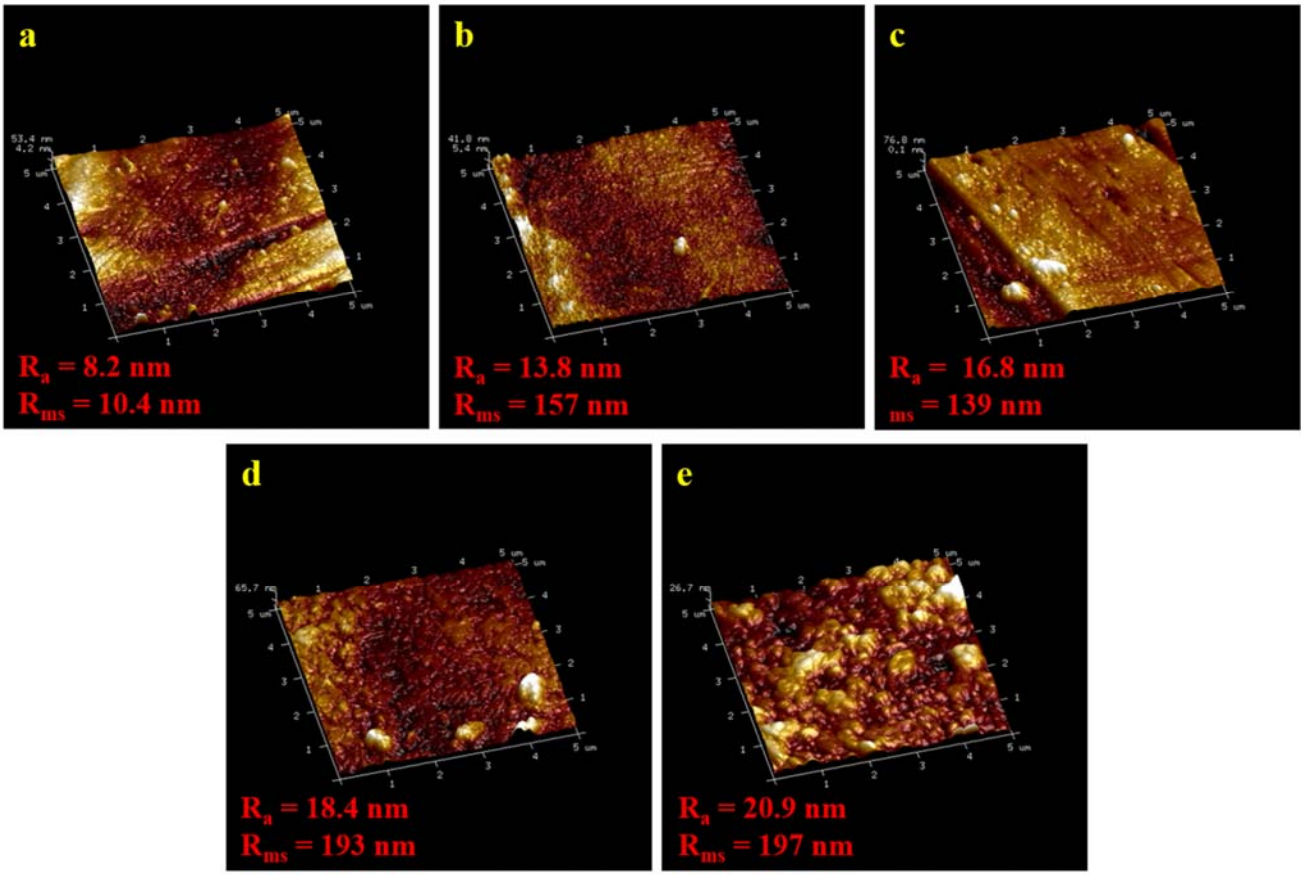

Fig. 7 Surface roughness of TFC and TFN membranes obtained by atomic force microscopy (AFM) analysis of (a) TFC, (b) TFN-0.01, (c) TFN-0.02, (d) TFN-0.05, and (e) TFN-0.1 PRO membranes.

3.4. Membrane intrinsic transport properties

PWP, as shown in Table 2**,** increased with SNW-1 loading, regardless whether COF material was introduced through MPD or TMC. This is highly consistent with the enhanced surface hydrophilicity observed earlier. Incorporation of a porous and highly-hydrophilic material, such as SNW-1, facilitates passage of water molecules through the composite membrane. Furthermore, similar to other TFN membranes in which nanoparticles are incorporated through the polyamide layer, the interface between the nanoparticles and the polymer also provides additional passageway for water to pass through [52, 62]. As expected, the high porosity of the nanoparticles does not only allow the passage of water molecules, but solute particle passage as well. This resulted in a significant increase in B (solute permeability coefficient) of the TFN membranes as compared to the TFC. Furthermore,

enhancement of membrane hydrophilicity brought about by SNW-1 incorporation significantly decreased the structural parameter *S* [37, 38, 54, 63].

Table 2 Intrinsic transport properties of the TFC and COF-incorporated TFN membranes.

Membrane	*A* (L m^{-2} h^{-1} bar^{-1})	*B* (L m^{-2} h^{-1})	*B/A* (bar)	R (%)	*S* (μm)
TFC	1.72	0.45	0.26	96.3	430
TFN-0.01	2.71	0.82	0.30	95.7	340
TFN-0.02	3.23	1.20	0.38	94.7	280
TFN-0.05	3.72	1.59	0.43	94.0	240
TFN-0.1	3.87	1.83	0.47	93.4	240
Toray PRO TFC	1.23	0.39	0.32	96.2	410

In comparison with the commercial PRO TFC membrane from Toray Chemicals, all the membranes prepared in this study showed better PWP. However, the commercial membrane exhibited better selectivity compared to the TFN membranes due to SNW-1, which did not just improve water permeability, but also reverse salt permeability.

3.5. PRO membrane performance

The PRO performance of the TFC and TFN membranes were evaluated by water flux (J_w), specific reverse salt flux (J_s/J_w), and power density, all of which are shown in Fig. and Fig. . The tests were performed using DI water and 1.0 M NaCl as feed and draw, respectively.

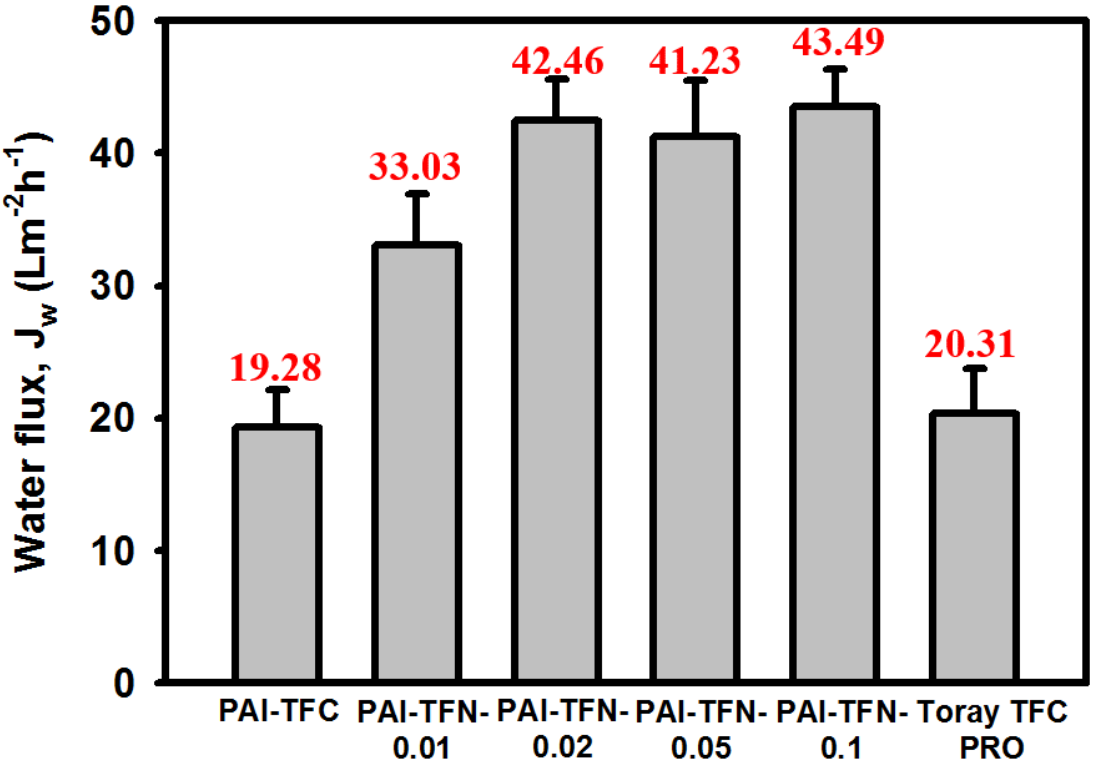

Fig. 8 Water flux (J_w) of the TFC and TFN PRO membranes in comparison with Toray TFC PRO membrane at 0 bar hydraulic pressure. (Feed solution: DI water; Draw solution: 1.0 M NaCl; Flow rate: 200 mL min^{-1})

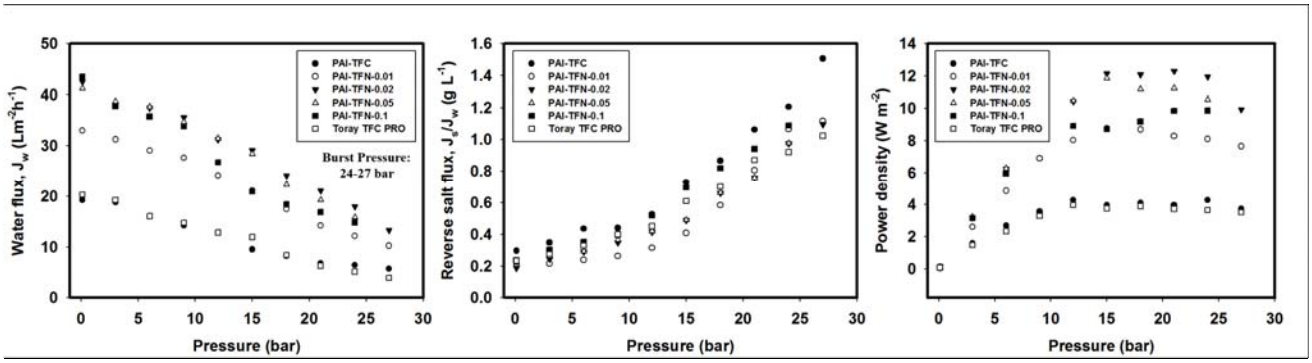

Fig. 9 Water flux (J_w), reverse salt flux (J_s), and power density of the membranes at various hydraulic pressures. (Feed solution: DI water; Draw solution: 1.0 M NaCl; Flow rate: 200 mL min^{-1})

As indicated by the PWP coefficients, water flux of the membranes improved significantly upon incorporation of the SNW-1 nanoparticles. Increasing the loading of SNW-1 allows the creation of more water-selective channels. This shows that enhancement of the membrane hydrophilicity would lead to enhanced membrane wetting and water transport [64]. This confirms that hydrophilicity plays a significant role in the enhancing the water flux and PRO membrane performance. Furthermore, SNW-1 has an ability to adsorb water molecules due to the H-bonding occurring between SNW-1's –NH functional groups and O-H of water. The enhanced hydrophilicity and selectivity of SNW-1 towards water molecule further enhance water continuity and transfer of water molecules across the membrane.

As mentioned earlier, the pores of SNW-1 have a major pore size of 5 Å, which is significantly larger than the size of the water molecule (3Å), thus it can easily allow water to pass through. Incorporation of SNW-1 in the dense polyamide layer simply provides free channels for water to pass through despite the dense property of polyamide. Furthermore, not only does the internal core of SNW-1 provide nanochannels for water transport, but also the gap between the interface of the nanomaterial and the polyamide allowed water transport to occur [65]. The enhanced fractional free volume due to the porous nanomaterials increases the membrane permeability. Although this can also undermine the membrane selectivity however, the size of the pores and the molecules, as well as the selectivity of SNW-1 towards water, take part in limiting reverse salt diffusion through the membranes [58]. The sieving property of the nanomaterial also comes into play, such that once water molecules have penetrated through the micro-sized pores of the COF material, no other molecule is able to penetrate further. Had the nanomaterial loading been increased further, aggregation of the particles may occur, which can lead to decreased permeability, due to blockage.

The water flux of the membranes was observed to decrease as the applied hydraulic pressures increased and it was a function of membrane compaction [66], as shown in Fig. 9. The compaction caused an increased effective membrane area resulted from stretching and thinning of the membrane polyamide selective layer [67]. The gradual decrease of water flux suddenly became a rapid increase at a point when the membranes have already sustained enough irreversible defects and damage, this point is known as the burst pressure. The highest J_w at $\Delta P=0$ bar was observed for TFN-0.1 (43.5 L m^{-2} h^{-1}), incorporated with 0.1 wt% SNW-1, marking a significant improvement as compared to water flux of

TFC (19.3 L m^{-2} h^{-1}). Even addition of 0.01 wt% of the COF increased the water flux to 33.0 L m^{-2} h^{-1} for TFN-0.01. It is, however, noticeable that the water flux did not follow a linear trend as SNW-1 loading increased, instead, a hyperbolic trend was observed. This is influenced by the membrane surface roughness, which offsets the enhanced hydrophilicity of the membranes. Moreover, the water fluxes of all TFN membranes with loading of at least 0.02 wt% SNW-1 are similar to each other. Thus, it can be suggested that 0.02 wt% is the optimum SNW-1 loading for future studies.

On the other hand, J_s/J_w of TFC-PRO membranes at $\Delta P=0$ bar were observed to increase as both SNW-1 loading and applied hydraulic pressure increase. These trends are consistent with the intrinsic properties of those TFC membranes from *A* and *B* values presented in Table 2. The results indicate that enhancement of hydrophilicity and porosity significantly enhanced both water and solute diffusivity. As hydraulic pressure increases, the membranes are subject to being damaged, which would cause more water and solute molecules to pass through.

The robustness of the membranes are evaluated by the burst pressure, or the pressure at which the membranes sustain damage. At this pressure, water and solute simply pass through the membrane. It is important to determine the burst pressure of membranes, especially for long-term PRO operation [68]. The membranes showed to have a burst pressure of 27 bar, except for TFN-0.05 and TFN-0.1, which burst at 24 bar. It is suggested that in future studies involving SNW-1-incorporated TFN membranes, pre-stabilization of the membranes at a pressure lower than the burst pressure must be performed prior to PRO operation to enhance the PRO performance of the membranes [69]. Furthermore, these results also indicate that higher loading of the SNW-1 nanomaterial can lead to instability of the membranes when operated for PRO at higher pressures, and 0.02 wt% of SNW-1 is the optimal loading at which the membranes can be operated at 27 bar. In the PRO process, a straightforward evaluation of membrane performance can be correlated with the power density (W m^{-2}). From Fig. , the maximum power density of 12.1 W m^{-2} at the pressure of 20 bar was achieved with TFN-M2, much higher than that obtained with the TFC membrane which was 4.28 W m^{-2}.

Conclusions

Novel PET open mesh fabric-reinforced SNW-1 covalent organic frameworks (COF)-incorporated thin film nanocomposite (TFN) pressure retarded osmosis (PRO) membranes were fabricated in this study. The mode of incorporation of SNW-1 was also investigated using two different precursors of the interfacial polymerization process. The following conclusions were drawn from this study:

1. Incorporation of the porous and hydrophilic nanomaterial resulted in significant enhancement of the surface hydrophilicity and water flux of the TFN membranes, due to the hydrophilic secondary amine functional groups of SNW-1;
2. The hydrophilicity and porosity of the nanomaterial facilitated the water transport across the membranes, while maintaining satisfactory salt rejection ability;
3. SNW-1 cannot be incorporated through TMC due to the reaction between the two, which is highly similar to that of polyamide formation;
4. Maximum pure water permeability was 3.87 $Lm^{-2}h^{-1}bar^{-1}$ for the membrane with 0.1 wt% SNW-1 incorporated through the MPD solution;
5. 0.02 wt% was considered to be the optimum loading of the nanomaterial, beyond which the loading affects the stability of the membrane at higher applied pressures; and
6. The highest water flux and power density for the membrane incorporated with 0.02 wt% SNW-1 through MPD were 42.5 $Lm^{-2}h^{-1}$ and 12.1 Wm^{-2} (at 20 bar), respectively.

These results indicate that the incorporation of a porous and hydrophilic COF nanomaterial such as SNW-1 is a promising method to fabricate high performance TFN PRO membranes.

ACKNOWLEDGMENT

This research was supported by a grant from the Qatar National Research Fund under its National Priorities Research Program award number NPRP 10-1231-160069 and the Australian Research Council (ARC) Future Fellowship (FT140101208).

References

[1] M.A. Shannon, P.W. Bohn, M. Elimelech, J.G. Georgiadis, B.J. Marinas, A.M. Mayes, Science and technology for water purification in the coming decades, Nature, 452 (2008) 301-310.

[2] G.M. Geise, H.-S. Lee, D.J. Miller, B.D. Freeman, J.E. McGrath, D.R. Paul, Water purification by membranes: The role of polymer science, Journal of Polymer Science Part B: Polymer Physics, 48 (2010) 1685-1718.

[3] T.-S. Chung, S. Zhang, K.Y. Wang, J. Su, M.M. Ling, Forward osmosis processes: Yesterday, today and tomorrow, Desalination, 287 (2012) 78-81.

[4] T.Y. Cath, A.E. Childress, M. Elimelech, Forward osmosis: Principles, applications, and recent developments: Review, Journal of Membrane Science, 281 (2006) 70-87.

[5] R.R. Gonzales, P. Sivagurunathan, S.-H. Kim, Effect of severity on dilute acid pretreatment of lignocellulosic biomass and the following hydrogen fermentation, International Journal of Hydrogen Energy, 41 (2016) 21678-21684.

[6] L.F. Greenlee, D.F. Lawler, B.D. Freeman, B. Marrot, P. Moulin, Reverse osmosis desalination: Water sources, technology, and today's challenges, Water Research, 43 (2009) 2317-2348.

[7] G. Han, S. Zhang, X. Li, T.-S. Chung, Progress in pressure retarded osmosis (PRO) membranes for osmotic power generation, Progress in Polymer Science, 51 (2015) 1-27.

[8] J. Kim, K. Jeong, M.J. Park, H.K. Shon, J.H. Kim, Recent advances in osmotic energy generation via pressure-retarded osmosis (PRO): A review, Energies, 8 (2015) 11821-11845.

[9] R.R. Gonzales, S.-H. Kim, Dark fermentative hydrogen production following the sequential dilute acid pretreatment and enzymatic saccharification of rice husk, International Journal of Hydrogen Energy, 42 (2017) 27577-27583.

[10] R.R. Gonzales, G. Kumar, P. Sivagurunathan, S.-H. Kim, Enhancement of hydrogen production by optimization of pH adjustment and separation conditions following dilute acid pretreatment of lignocellulosic biomass, International Journal of Hydrogen Energy, 42 (2017) 27502-27511.

[11] R.R. Gonzales, P. Sivagurunathan, A. Parthiban, S.-H. Kim, Optimization of substrate concentration of dilute acid hydrolyzate of lignocellulosic biomass in batch hydrogen production, International Biodeterioration and Biodegradation, 113 (2016) 22-27.

[12] T.-S. Chung, X. Li, R.C. Ong, Q. Ge, H. Wang, G. Han, Emerging forward osmosis (FO) technologies and challenges ahead for clean water and clean energy applications, Current Opinion in Chemical Engineering, 1 (2012) 246-257.

[13] L. Chekli, S. Phuntsho, H.K. Shon, S. Vigneswaran, J. Kandasamy, A. Chanan, A review of draw solutes in forward osmosis process and their use in modern applications, Desalination and Water Treatment, 43 (2012) 167-184.

[14] S. Phuntsho, H.K. Shon, T. Majeed, I. El Saliby, S. Vigneswaran, J. Kandasamy, S. Hong, S. Lee, Blended fertilizers as draw solutions for fertilizer-drawn forward osmosis desalination, Environmental Science & Technology, 46 (2012) 4567-4575.

[15] D.I. Kim, J. Kim, H.K. Shon, S. Hong, Pressure retarded osmosis (PRO) for integrating seawater desalination and wastewater reclamation: Energy consumption and fouling, Journal of Membrane Science, 483 (2015) 34-41.

[16] A. Achilli, T.Y. Cath, A.E. Childress, Power generation with pressure retarded osmosis: An experimental and theoretical investigation, Journal of Membrane Science, 343 (2009) 42-52.

[17] T.-S. Chung, L. Luo, C.F. Wan, Y. Cui, G. Amy, What is next for forward osmosis (FO) and pressure retarded osmosis (PRO), Separation and Purification Technology, 156 (2015) 856-860.

[18] Q. She, X. Jin, C.Y. Tang, Osmotic power production from salinity gradient resource by pressure retarded osmosis: Effects of operating conditions and reverse solute diffusion, Journal of Membrane Science, 401 (2012) 262-273.
[19] N.Y. Yip, M. Elimelech, Performance limiting effects in power generation from salinity gradients by pressure retarded osmosis, Environmental Science & Technology, 45 (2011) 10273-10282.
[20] A.P. Straub, C.O. Osuji, T.Y. Cath, M. Elimelech, Selectivity and mass transfer limitations in pressure-retarded osmosis at high concentrations and increased operating pressures, Environmental Science & Technology, 49 (2015) 12551-12559.
[21] C. Klaysom, T.Y. Cath, T. Depuydt, I.F.J. Vankelecom, Forward and pressure retarded osmosis: potential solutions for global challenges in energy and water supply, Chemical Society Reviews, 42 (2013) 6959-6989.
[22] A.P. Straub, A. Deshmukh, M. Elimelech, Pressure-retarded osmosis for power generation from salinity gradients: is it viable?, Energy & Environmental Science, 9 (2016) 31-48.
[23] F. Volpin, R.R. Gonzales, S. Lim, N. Pathak, S. Phuntsho, H.K. Shon, GreenPRO: A novel fertiliser-driven osmotic power generation process for fertigation, Desalination, 447 (2018) 158-166.
[24] N.Y. Yip, A. Tiraferri, W.A. Phillip, J.D. Schiffman, L.A. Hoover, Y.C. Kim, M. Elimelech, Thin-film composite pressure retarded osmosis membranes for sustainable power generation from salinity gradients, Environmental Science & Technology, 45 (2011) 4360-4369.
[25] G. Han, P. Wang, T.-S. Chung, Highly robust thin-film composite pressure retarded osmosis (PRO) hollow fiber membranes with high power densities for renewable salinity-gradient energy generation, Environmental Science & Technology, 47 (2013) 8070-8077.
[26] P.G. Ingole, W. Choi, K.-H. Kim, H.-D. Jo, W.-K. Choi, J.-S. Park, H.-K. Lee, Preparation, characterization and performance evaluations of thin film composite hollow fiber membrane for energy generation, Desalination, 345 (2014) 136-145.
[27] L. Huang, J.T. Arena, M.T. Meyering, T.J. Hamlin, J.R. McCutcheon, Tailored multi-zoned nylon 6,6 supported thin film composite membranes for pressure retarded osmosis, Desalination, 399 (2016) 96-104.
[28] A. Tiraferri, N.Y. Yip, W.A. Phillip, J.D. Schiffman, M. Elimelech, Relating performance of thin-film composite forward osmosis membranes to support layer formation and structure, Journal of Membrane Science, 367 (2011) 340-352.
[29] J. Wei, C. Qiu, C.Y. Tang, R. Wang, A.G. Fane, Synthesis and characterization of flat-sheet thin film composite forward osmosis membranes, Journal of Membrane Science, 372 (2011) 292-302.
[30] I. Alsvik, M.-B. Hägg, Pressure retarded osmosis and forward osmosis membranes: Materials and methods, Polymers, 5 (2013) 303.
[31] A.P. Straub, S. Lin, M. Elimelech, Module-scale analysis of pressure retarded osmosis: Performance limitations and implications for full-scale operation, Environmental Science & Technology, 48 (2014) 12435-12444.
[32] H.-g. Choi, M. Son, H. Choi, Integrating seawater desalination and wastewater reclamation forward osmosis process using thin-film composite mixed matrix membrane with functionalized carbon nanotube blended polyethersulfone support layer, Chemosphere, 185 (2017) 1181-1188.
[33] B. Zornoza, C. Tellez, J. Coronas, J. Gascon, F. Kapteijn, Metal organic framework based mixed matrix membranes: An increasingly important field of research with a large application potential, Microporous and Mesoporous Materials, 166 (2013) 67-78.

[34] L. Wang, X. Song, T. Wang, S. Wang, Z. Wang, C. Gao, Fabrication and characterization of polyethersulfone/carbon nanotubes (PES/CNTs) based mixed matrix membranes (MMMs) for nanofiltration application, Applied Surface Science, 330 (2015) 118-125.
[35] M. Amini, M. Jahanshani, A. Rahimpour, Synthesis of novel thin film nanocomposite (TFN) forward osmosis membranes using functionalized multi-walled carbon nanotubes, Journal of Membrane Science, 435 (2013) 233-241.
[36] D. Emadzadeh, W.J. Lau, A.F. Ismail, Synthesis of thin film nanocomposite forward osmosis membrane with enhancement in water flux without sacrificing salt rejection, Desalination, 330 (2013) 90-99.
[37] S. Lim, M.J. Park, S. Phuntsho, L.D. Tijing, G.M. Nisola, W.-G. Shim, W.-J. Chung, H.K. Shon, Dual-layered nanocomposite substrate membrane based on polysulfone/graphene oxide for mitigating internal concentration polarization in forward osmosis, Polymer, 110 (2017) 36-48.
[38] M.J. Park, S. Phuntsho, T. He, G.M. Nisola, L.d. Tijing, X.-M. Li, G. Chen, W.-J. Chung, H.K. Shon, Graphene oxide incorporated polysulfone substrate for the fabrication of flat-sheet thin-film composite forward osmosis membranes, Journal of Membrane Science, 493 (2015) 496-507.
[39] Y. Wang, R. Ou, H. Wang, T. Xu, Graphene oxide modified graphitic carbon nitride as a modifier for thin film composite forward osmosis membrane, Journal of Membrane Science, 475 (2015) 281-289.
[40] A. Soroush, W. Ma, Y. Silvino, M.S. Rahaman, Surface modification of thin film composite forward osmosis membrane by silver-decorated graphene-oxide nanosheets, Environmental Science: Nano, 2 (2015) 395-405.
[41] N. Ma, J. Wei, R. Liao, C.Y. Tang, Zeolite-polyamide thin film nanocomposite membranes: Towards enhanced performance for forward osmosis, Journal of Membrane Science, 405 (2012) 149-157.
[42] Y. Wang, R. Ou, Q. Ge, H. Wang, T. Xu, Preparation of polyethersulfone/carbon nanotube substrate for high-performance forward osmosis membrane, Desalination, 330 (2013) 70-78.
[43] M. Tian, Y.-N. Wang, R. Wang, Synthesis and characterization of novel high-performance thin film nanocomposite (TFN) FO membranes with nanofibrous substrate reinforced by functionalized carbon nanotubes, Desalination, 370 (2015) 79-86.
[44] D. Emadzadeh, W.J. Lau, T. Matsuura, M. Rahbari-Sisakht, A.F. Ismail, A novel thin film composite forward osmosis membrane prepared from PSf-TiO2 nanocomposite substrate for water desalination, Chemical Engineering Journal, 237 (2014) 70-80.
[45] D. Emadzadeh, W.J. Lau, T. Matsuura, A.F. Ismail, M. Rahbari-Sisakht, Synthesis and characterization of thin film nanocomposite forward osmosis membrane with hydrophilic nanocomposite support to reduce internal concentration polarization, Journal of Membrane Science, 449 (2014) 74-85.
[46] M. Tian, Y.-N. Wang, R. Wang, A.G. Fane, Synthesis and characterization of thin film nanocomposite forward osmosis membranes supported by silica nanoparticle incorporated nanofibrous substrate, Desalination, 401 (2017) 142-150.
[47] X. Gao, X. Zou, H. Ma, S. Meng, G. Zhu, Highly selective and permeable porous organic framework membrane for CO2 capture, Advanced Materials, 26 (2014) 3644-3648.
[48] S. Sorribas, P. Gorgojo, C. Téllez, J. Coronas, A.G. Livingston, High flux thin film nanocomposite membranes based on metal-organic frameworks for organic solvent nanofiltration, Journal of the American Chemical Society, 135 (2013) 15201-15208.
[49] I. Tiscornia, I. Kumakiri, R. Bredesen, C. Téllez, J. Coronas, Microporous titanosilicate ETS-10 membrane for high pressure CO2 separation, Separation and Purification Technology, 73 (2010) 8-12.

[50] S. Kitagawa, R. Kitaura, S.-i. Noro, Functional porous coordination polymers, Angewandte Chemie International Edition, 43 (2004) 2334-2375.
[51] S.-Y. Ding, W. Wang, Covalent organic frameworks (COFs): From design to applications, Chemical Society Reviews, 42 (2013) 548-568.
[52] C. Wang, Z. Li, J. Chen, Z. Li, Y. Yin, L. Cao, Y. Zhong, H. Wu, Covalent organic framework modified polyamide nanofiltration membrane with enhanced performance for desalination, Journal of Membrane Science, 523 (2017) 273-281.
[53] M.G. Schwab, B. Fassbender, H.W. Spiess, A. Thomas, X. Feng, K. Müllen, Catalyst-free preparation of melamine-based microporous polymer networks through Schiff Base chemistry, Journal of the American Chemical Society, 131 (2009) 7216-7217.
[54] M.J. Park, R.R. Gonzales, A. Abdel-Wahab, S. Phuntsho, H.K. Shon, Hydrophilic polyvinyl alcohol coating on hydrophobic electrospun nanofiber membrane for high performance thin film composite forward osmosis membrane, Desalination, 426 (2018) 50-59.
[55] R.R. Gonzales, J.M. Park, L. Tijing, S.D. Han, S. Phuntsho, K.H. Shon, Modification of nanofiber support layer for thin film composite forward osmosis membranes via layer-by-layer polyelectrolyte deposition, Membranes, 8 (2018).
[56] S. Qiu, L. Wu, L. Zhang, H. Chen, C. Gao, Preparation of reverse osmosis composite membrane with high flux by interfacial polymerization of MPD and TMC, Journal of Applied Polymer Science, 112 (2009) 2066-2072.
[57] S. Belfer, Y. Purinson, O. Kedem, Surface modification of commercial polyamide reverse osmosis membranes by radical grafting: An ATR-FTIR study, Acta Polymerica, 49 (1998) 574-582.
[58] H. Yang, H. Wu, F. Pan, Z. Li, H. Ding, G. Liu, Z. Jiang, P. Zhang, X. Cao, B. Wang, Highly water-permeable and stable hybrid membrane with asymmetric covalent organic framework distribution, Journal of Membrane Science, 520 (2016) 583-595.
[59] S. Chou, R. Wang, L. Shi, Q. She, C. Tang, A.G. Fane, Thin-film composite hollow fiber membranes for pressure retarded osmosis (PRO) process with high power density, Journal of Membrane Science, 389 (2012) 25-33.
[60] N.-N. Bui, J.R. McCutcheon, Nanofiber supported thin-film composite membrane for pressure-retarded osmosis, Environmental Science & Technology, 48 (2014) 4129-4136.
[61] T.-Y. Liu, H.-G. Yuan, Y.-Y. Liu, D. Ren, Y.-C. Su, X. Wang, Metal-organic framework nanocomposite thin films with interfacial bindings and self-standing robustness for high water flux and enhanced ion selectivity, ACS Nano, (2018).
[62] J. Yin, E.-S. Kim, J. Yang, B. Deng, Fabrication of a novel thin-film nanocomposite (TFN) membrane containing MCM-41 silica nanoparticles (NPs) for water purification, Journal of Membrane Science, 423-424 (2012) 238-246.
[63] J.T. Arena, B. McCloskey, B.D. Freeman, J.R. McCutcheon, Surface modification of thin film composite membrane support layers with polydopamine: Enabling use of reverse osmosis membranes in pressure retarded osmosis, Journal of Membrane Science, 375 (2011) 55-62.
[64] C. Liu, X. Li, T. Liu, Z. Liu, N. Li, Y. Zhang, C. Xiao, Microporous CA/PVDF membranes based on electrospun nanofibers with controlled crosslinking induced by solvent vapor, Journal of Membrane Science, 2016 (2016) 1-12.
[65] Y. Li, Y. Zhao, E. Tian, Y. Ren, Preparation and characterization of novel forward osmosis membrane incorporated with sulfonated carbon nanotubes, RSC Advances, 8 (2018) 41032-41039.
[66] G. Han, T.-S. Chung, Robust and high performance pressure retarded osmosis hollow fiber membranes for osmotic power generation, AIChE Journal, 60 (2014) 1107-1119.
[67] Y. Choi, S. Vigneswaran, S. Lee, Evaluation of fouling potential and power density in pressure retarded osmosis (PRO) by fouling index, Desalination, 389 (2016) 215-223.

[68] Y. Chen, L. Setiawan, S. Chou, X. Hu, R. Wang, Identification of safe and stable operation conditions for pressure retarded osmosis with high performance hollow fiber membrane, Journal of Membrane Science, 503 (2016) 90-100.
[69] W. Gai, X. Li, J.Y. Xiong, C.F. Wan, T.-S. Chung, Evolution of micro-deformation in inner-selective thin film composite hollow fiber membranes and its implications for osmotic power generation, Journal of Membrane Science, 516 (2016) 104-112.